Experimental Study of Ion Dynamic Effects in Overlapping Helium Lines at Low Densities

A. Piel and H. Richter
Institut für Experimentalphysik II der Ruhr-Universität Bochum

Z. Naturforsch. **38 a**, 37–46 (1983); received September 29, 1982

The line profiles of the overlapping helium lines 447.1 nm and 492.2 nm have been investigated in an improved plasma source of high purity at electron densities of 1×10^{21} m^{-3} and 3×10^{21} m^{-3}. The plasma parameters N_e, T_e and T_0 were determined carefully by independent diagnostics, which enables a critical comparison with existing theories (BCS II and MMM). We observed ion dynamic effects which considerably modify the line shape of the forbidden components. Our experiments extend the existing observations towards higher ion temperatures. Systematic trends observed earlier are critically discussed.

Introduction

During the last decade several experimental and theoretical approaches have been made to study ion dynamic effects in the Stark broadening of hydrogen and helium spectral lines. The term "ion dynamics" was created by Burgess [1] who concluded from the experimental findings of Burgess and Cairns [2] that the discrepancies in the intensity of the forbidden component $2\,^3P-4\,^3F$ of the helium line at 447 nm as compared with the theories of Griem [3] and Barnard et al. [4] (BCS I) are due to the quasistatic treatment of the ions in these theories. The quasistatic approximation, however, breaks down within a frequency separation from the center of the forbidden line of the order of the Weisskopf frequency. Improved calculations for the HeI $\lambda = 447$ nm line of Barnard et al. [5] (BCS II) show that the inclusion of ion motion leads to a considerable modification of the forbidden line profile resulting in a closer agreement with the experimental findings.

At present there are three different theoretical approaches, the theory of Lee [6, 7], the Unified Theory (BSC II) and the Model Microfield Method (MMM) [8, 9], which exhibit measurable differences in the description of the helium lines with overlapping forbidden components. The fundamental difference between the latter two theories lies in the fact that the Unified Theory starts from a particle picture, while the MMM incorporates the statistical properties of the plasma microfield only. Lee's result is similar to BCS II, whereas ion dynamic corrections to BCS I calculated by Voslamber and Segré [10] nearly coincide with MMM.

Ion dynamic effects depend on the relative velocity between the perturbing ion and the radiating atom, which is a function of the ion temperature T_i and the reduced mass μ of the radiator-perturber system. Consequently two different ways of varying the ion velocity have been applied in earlier experiments. The mass of the perturbing ion was changed in the plasma-jet of Fleurier et al. [11, 12]. The ion temperature was varied using nonequilibrium effects in helium arcs by Helbig and Ehrich [13]. Both investigations result in a systematic dependence on $(T_i/\mu)^{1/2}$, which is in general agreement with the predictions of MMM [14].

Besides this general agreement there are some remaining unexplained tendencies which might have an experimental origin. This situation stimulated a careful reexamination of ion dynamic effects in helium lines. Therefore we have developed an improved plasma device, which enables accurate and independent diagnostics of all relevant plasma parameters. In addition the ion temperatures in our discharge were increased towards higher values, exceeding those in the experiments of Helbig and Ehrich. Hereby the temperature dependent trends could be studied in an extended range.

I. Experimental Arrangement and Generation of Pure Helium Spectra

The construction of pulsed linear discharges for spectroscopic purposes dates back to the work of

Reprint requests to Dr. A. Piel, Institut für Experimentalphysik II der Ruhr-Universität Bochum, Postfach 10 21 48, D-4630 Bochum.

0340-4811 / 83 / 0100-0037 $ 01.3 0/0. – Please order a reprint rather than making your own copy.

Wulff [15], who developed a highly ionized helium arc plasma produced in a closed quartz tube by applying a pulsed current of a few thousand ampères. This device was subsequently used for line profile studies of both atomic and ionized helium lines [16, 17]. A thorough investigation of the Stark broadening of the helium line $2\,^3P-4\,^3D$, ^3F at $\lambda = 447.1$ nm at low electron densities was performed by Drawin and Ramette [18, 19], who employed the afterglow of such a pulsed discharge. The present work has been performed on an improved version of this kind of discharge during the burning phase.

1. Discharge Tube and Electrical Circuit

A detailed sketch of our experimental arrangement is shown in Figure 1. The discharge tube consists of a cylindrical section (433 mm long, 25 mm i.d.), which is axially terminated by plane quartz windows, and of two annular sections containing ring shaped tungsten electrodes at both ends. The entire discharge tube is made of fused quartz.

It has been demonstrated earlier by the authors [20, 21] that hydrogen impurities arising from a water layer on the inner wall of the discharge tube considerably modify helium discharges. For reducing the water content the whole tube can be heated to 400 °C continuously by means of a heater coil, which simultaneously serves as an antenna for producing a RF-discharge. An oil free vacuum is provided by a turbomolecular pump and the discharge tube can be sealed by a quartz valve. The discharge circuit has been designed as an overcritically damped LC circuit. The inductance has been

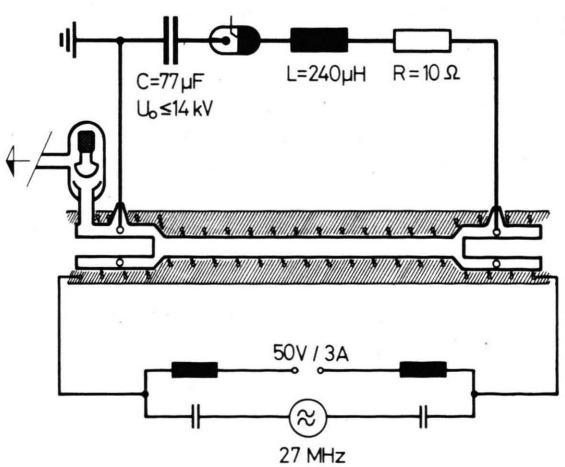

Fig. 1. Discharge tube and electrical circuit.

introduced mainly for reducing dN_e/dt at ignition facilitating the monitoring of interferometer fringes during the discharge build-up. Since the voltage drop across the discharge tube is much less than that across the external network, the discharge current is determined completely by the RLC circuit and the initial voltage of the capacitor. This ensures an excellent reproducibility of the discharge.

2. Optical Arrangement

Figure 2 shows the optical arrangement. The plasma light is observed end-on through a set of apertures, which limit the volume under observation to a 4 mm dia. cylinder centered on the tube axis. By omitting the mirror M5 the same source volume can be diagnosed by a laser interferometer. The interferometer utilizes the feedback of the beam into the laser resonator [22, 23] after passing 2, 4 or 6 times through the plasma, which is accomplished by tilting the mirrors M3 and M4. The interferometer fringes are observed monitoring the laser output power on either 3.39 µm or 0.633 µm. The entire arrangement is mounted on a granite table.

Different spectrometers have been applied to this plasma source. The line profiles of the HeI 447.1 nm and 492.2 nm lines were recorded with a lm Czerny Turner instrument with a 1200 grooves/mm grating and an optical multichannel analyzer (PAR 1205 D). The Doppler broadening of HeI 388.8 nm was measured using a 2 m Zeiss intrument in Ebert mounting with a low instrument width of 6 pm. Integral line intensities in the violet and the near UV could be recorded with a quartz prism spectrometer. More details of the spectroscopic arrangement can be found in [24].

3. Reduction of Impurities

It was demonstrated in earlier observations [21] that hydrogen impurities lead to a nonnegligible intensity of molecular lines and a quasicontinuum of merging lines even in pulsed discharges. This kind of impurity radiation may considerably alter the line shape in the vicinity of the "forbidden component" of the 447.1 nm and 492.2 nm lines. Therefore the efficiency of the cleaning procedure was monitored by observing the H_β line intensity, which is a sensitive indicator for residual hydrogen. In a tube with cold walls, which has been exposed to

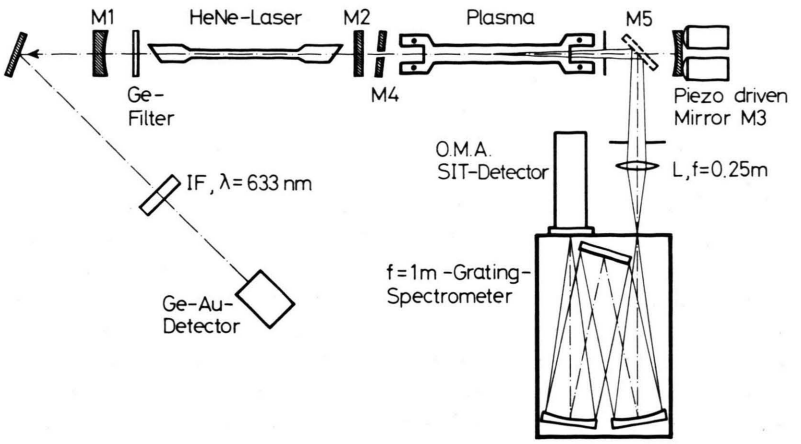

Fig. 2. Optical arrangement and laser interferometer.

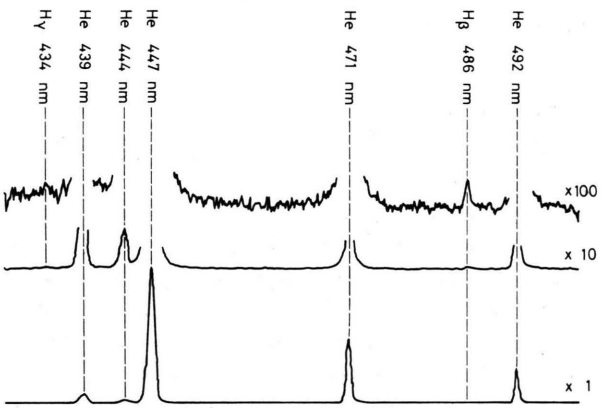

Fig. 3. The residual intensity of H_β in a heated tube.

moist air and has been evacuated for more than 24 hours, the intensity of H_β is nevertheless comparable to that of 447.1 nm. This statement holds for both a stationary RF-discharge and for the pulsed arc discharge. By heating the tube walls during evacuation H_β can be reduced by two orders of magnitude, which is shown in Figure 3. Additional impurity radiation may arise from the materials of the wall and of the electrodes. These elements such as silicon, oxygen and tungsten were identified by their characteristic lines, but these weak lines did not interfere with the line profiles of interest.

II. Determination of the Plasma Parameters

For a quantitative comparison between measured and calculated line profiles the parameters electron density N_e, electron temperature T_e, ion temperature T_i and gas temperature T_0 must be determined with sufficient accuracy. It is the advantage of these investigations that all these parameters are measured by methods which are independent of the Stark broadening of the helium lines.

1. Electron Density

The electron density is determined from the refractivity of the plasma. At the low pressure of 100 to 400 Pa used here the refractivity is entirely due to the free electrons. Since the positive column of this arc was proved to be sufficiently homogeneous in axial direction [18] we are permitted to deduce the electron density immediately from the line integrated refractivity. The multiple path of the laser beam was confined to a central region of less than 6 mm diameter. Therefore the radial density profile

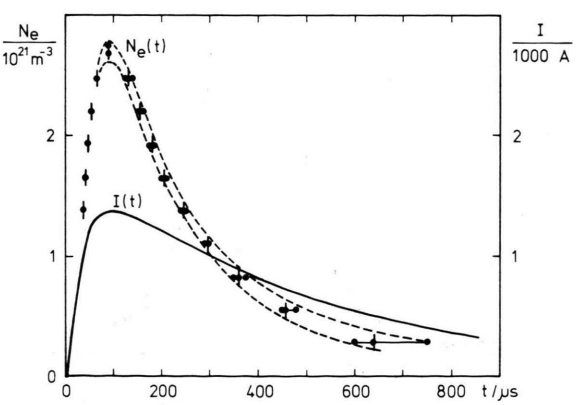

Fig. 4. Discharge current and electron density.

could be neglected. The He-Ne laser simultaneously operates on the red (0.633 μm) and the infrared wavelength (3.39 μm), which are coupled by their common upper state. Interferometric fringes can therefore be observed either directly on the IR-wavelength or as a modulation of the red wavelength in the "Ashby-Jephcott Mode" [22]. For the adjustment of the feed-back fringes are produced by the vibrating mirror M 3.

The shot to shot reproducibility of the interferometer can immediately be read from the scatter of three independent shots in Figure 4. The relative error of N_e primarily arises from the uncertainty of fixing the phase at the end of the discharge, which introduces a quarter fringe error. It can be seen that all three measurements fall into this intervall. At six passes through the plasma the sensitivity is $2.54 \times 10^{20}\,m^{-3}$ per fringe, which results in an accuracy of 6% at the lowest density of interest ($1 \times 10^{21}\,m^{-3}$). The electron density can be considered as sufficiently constant during 50 μs around the maximum.

We have also compared our interferometric measuremets with the halfwidth of H_β, which was used as N_e diagnostics in [13]. For this purpose the discharge was operated in pure hydrogen. The measured profile of H_β is shown in Figure 5. For comparison a theoretical profile according to Seidel's MMM calculations [25–27] is shown, which contains a convolution with our instrument profile. Although the central minimum of H_β is sensitive to ion dynamic effects, the halfwidth is sufficiently unaffected as was pointed out by Ehrich and Helbig [28]. The central dip of H_β is filled up in our experimental line profile. We attribute this to a residual radiation from a low density layer at the end window and to molecular radiation of H_2. The experimental and theoretical profiles show a close agreement in the halfwidth and in the line wings. From this comparison it can be concluded that determining N_e from the halfwidth of H_β, which is a well established method at higher electron densities, yields a reliable result even at $N_e = 10^{21}\,m^{-3}$, which agrees with interferometry within an estimated error of about 10%.

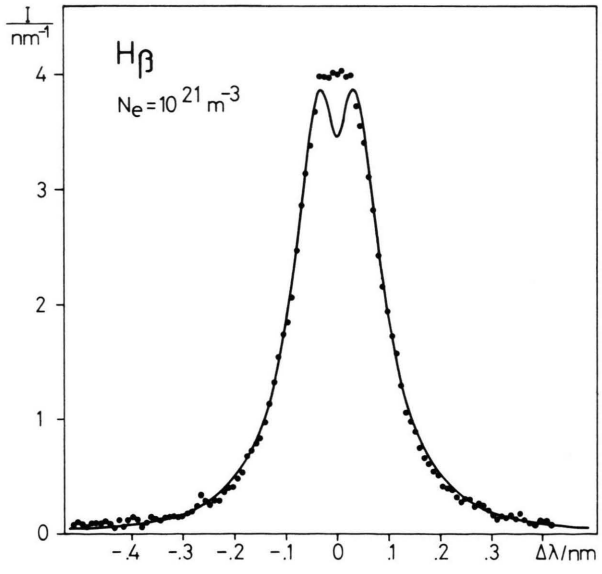

Fig. 5. The line profile of H_β in comparison with Seidel's MMM calculation.

2. *Gas Temperature*

The temperatures of the ions and neutrals, which are assumed to be equal, can be derived from the Doppler broadening ob those spectral lines, which have a negligible Stark broadening. Since the Dopplereffect decreases with increasing atomic mass helium lines are preferred. According to the Stark broadening parameters given by Griem [29] the He I line at 388.9 nm was selected, which in addition is a rather strong line. The line profile was recorded using a $f = 2$ m Zeiss Jena plane grating spectrometer in Ebert mounting, which provides a narrow instrument width. Due to the large focal length and the high dispersion, however, this instrument possesses a low sensitivity. It was necessary to count single photomultiplier pulses during the 50 μs of constant plasma parameters around the density maximum. Typical counting rates were about 700 in the line center. The optical depth of the line was measured by the usual concave mirror method and turned out to be negligible, as can be seen from the identical line shapes in Figure 6.

The line profiles have been normalized to unity area and theoretical line profiles have been calculated as follows: The instrument profile measured with a Hg 115 microwave lamp was folded with the Stark profile according to Griem's [29] formulae, which involves the actual electron density of $3 \times 10^{21}\,m^{-3}$. Subsequently this profile was folded with Gaussian profiles of different temperatures and the whole profile was area normalized. One can

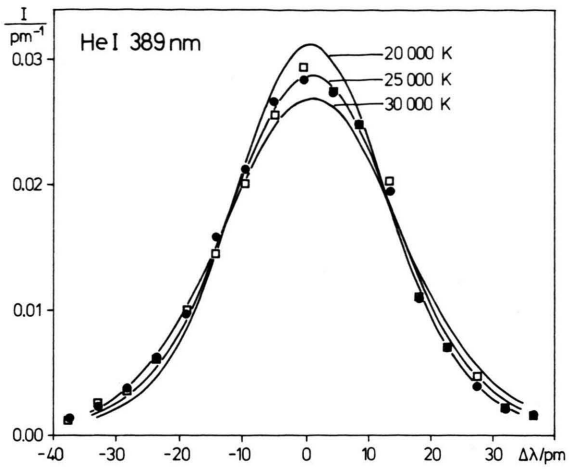

Fig. 6. HeI 388.9 nm compared with calculated profiles at different temperatures. Dots and squares corresponds to measurements without and with the concave mirror.

immediately read from Fig. 6 that the temperature of best fit is 25000 K and the estimated error amounts to 5000 K. At the lower electron density of 1×10^{21} m^{-3} the gas temperature was found to be 15000 K ± 3000 K. Using improved Stark profiles, including ion dynamics, which we have calculated according to BCS II, the gas temperatures were 15000 K at 1×10^{21} m^{-3} and 21000 K at 3×10^{21} m^{-3}, which lie within the error bars given above.

3. *Electron Temperature*

The electron temperature can be derived from relative line intensities if a reasonable assumption about the plasma equilibrium can be made. For levels close to the ionization limit the population is given by the Saha-Boltzmann relation [30] since partial local thermodynamic equilibrium is maintained by electron collisions. This can be expected for principal quantum numbers $n > 5$ at our conditions. Nevertheless this method is very sensitive to experimental errors. Due to the small difference of term energies (0.25 eV) involved here there is only a weak variation of the exponential $\exp(-\Delta E/kT)$ between 20000 K and 30000 K. On the other hand the line intensity measurement can be falsified by an erroneous calibration. It is therefore not surprising that this method yields an arbitrary value for T_e. The same conclusion was drawn by Burgess and Cairns [2], who reported even negative temperatures by this method under comparable conditions.

More reliable temperature measurements can be obtained from line intensities involving different ionization stages of the same element. Griem [30] proposed to use the ratio of HeII 468.6 nm/HeI 587.6 nm, but the latter turned out to be optically thick in our case. We therefore applied the same model to the line pair HeII 468.6 nm/HeI 471.3 nm, which can be recorded simultaneously on the OMA. Thus no corrections for the sensitivity had to be made. According to Griem's model the atomic and ionic levels are related to the next higher ionization stage by LTE, but the ratio of He^{++}/He^{+} is calculated from the collisional radiative model (CR) of Bates *et al.* [31].

In addition we have also investigated the line to continuum ratio at 471.3 nm and the ratio of oxygen lines OII 436.69 nm/OI 436.83 nm. All results are compiled in Table 1.

At the lower density of 1×10^{21} m^{-3} the collisional radiative model depends on only two tabulated values for S/α which require an interpolation over 9 orders of magnitude. Therefore we have also calculated the temperature assuming LTE between He^{++} and H^{+}, which results in a lower limit for T_e at 19000 K. The oxygen lines and the line to continuum ratio give a slightly higher temperature. The most probable value for T_e is 20000 K, which exceeds the gas temperature by 5000 K. A similar difference between electron and gas temperature has been reported by Fleurier et al. [11].

At the higher density only the CR-model and the line to continuum method yielded reliable results. Both methods confirm each other and the resulting temperature of $T_e = 31000$ K shows a similar deviation from the gas temperature. It should be stressed that the electron temperature has only a weak influence on the line shapes to be discussed below.

Table 1.

Method	T_e/K at N_e =	
	1×10^{21} m^{-3}	3×10^{21} m^{-3}
Boltzmann plot	(5 000)	–
HeII468.6/HeI471.3 CR-Model	28 000	31 000
HeII468.6/HeI471.3 Saha-Model	19 000	–
OII436.69/OI436.83	20 000	–
HeI471.3/continuum	20 000	31 000
Gas Temperature	15 000	25 000

Table 2.

Quantity	Set 1	Set 2	Unit
p_{He}	100	400	Pa
I_{max}	1 000	1 400	A
$N_{e,\,max}$	1×10^{21}	3×10^{21}	m^{-3}
$T_o = T_i$	15 000	25 000	K
T_e	20 000	31 000	K

4. Discharge Conditions

Our low pressure arc can be operated at electron densities from $10^{20}\,m^{-3}$ to $3\times10^{22}\,m^{-3}$ by varying the discharge current and the helium pressure. For the present investigations only two sets of discharge conditions have been selected, which are compiled in Table 2 together with the results of the diagnostics described above. The electron density was chosen to be either $1\times10^{21}\,m^{-3}$ or $3\times10^{21}\,m^{-3}$. For these values tabulated line profiles were available. Smaller electron densities would lead to errors exceeding 10% in the independent N_e measurement. At larger electron densities the differences between the static and dynamic calculations gradually vanish.

III. Line Profile Measurements

1. Comparison of Different Theories

The line shapes of the forbidden component of HeI 447.1 nm according to four different theoretical calculations are compiled in Figure 7. The curve labelled BCS I represents the limiting case of static ions ($T_i = 0$). The influence of ion motion leads to a general reduction in the intensity of the forbidden component, which is most pronounced for the Unified Theory (BSC II) and the theory of Lee that nearly coincides with BCS II. Simultaneously the "valley" between the allowed and forbidden component is filled up. Basically the same tendency is also found in the MMM calculations. But in addition the forbidden component is slightly narrower and shifted to the allowed line. Voslamber and Segrè have also calculated dynamic corrections to BCS I, which show an intensity and shift comparable to MMM.

Although ion dynamic corrections mainly alter the forbidden component and the transition region the entire line profile has to be compared with the experiment owing to the modification of the allowed line by area normalization. In order to show the weak influence of an experimental error in the electron density we have drawn the MMM profile at $N_e = 1\times10^{21}\,m^{-3} \pm 10\%$ (Figure 8). Surprisingly the peak intensity of the forbidden component and the intensity of the valley are nearly unchanged because

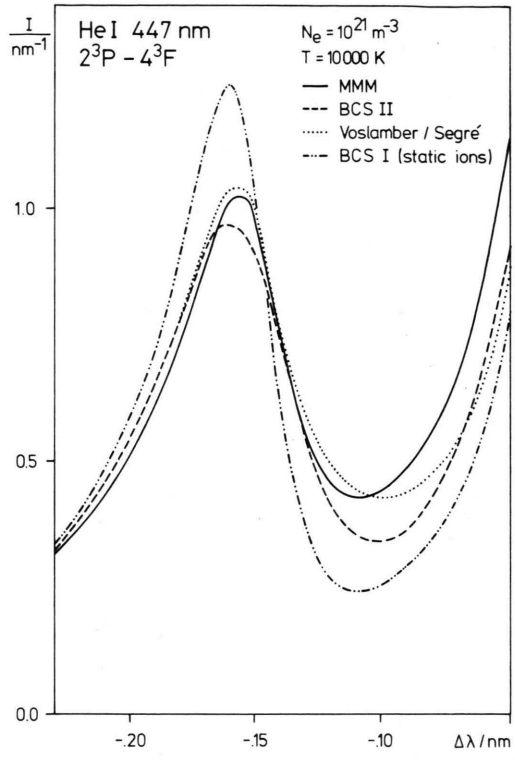

Fig. 7. The forbidden component of HeI 447.1 nm according to different theories.

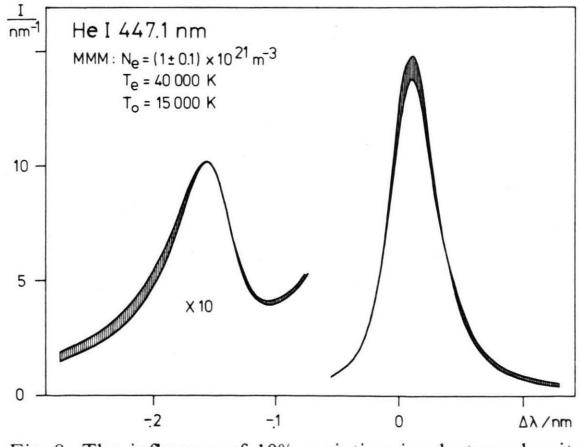

Fig. 8. The influence of 10% variation in electron density on the calculated profile according to MMM.

of the counteracting effects of broadening and area normalization. The intensity of the allowed line, however, reflects the changes in the line wings. Therefore the existing differences in the theories as shown in Fig. 12 are not destroyed by the remaining uncertainty of N_e. The other plasma parameters possess even weaker influences on the line profile.

2. Results and Conclusions

In the following a comparison will be made with BCS II and MMM, because only for these theories tabulated line profiles for both the 447.1 nm and the 492.2 nm line were available to us. The static profile according to BCS I has been omitted from the subsequent figures for clarity. The drastic deviation of all experimental profiles from the static profile can be read from Figure 7. Calculated line profiles at the actual electron and ion temperatures are finally folded with our instrument profile and area normalized for a direct comparison with the measured profile.

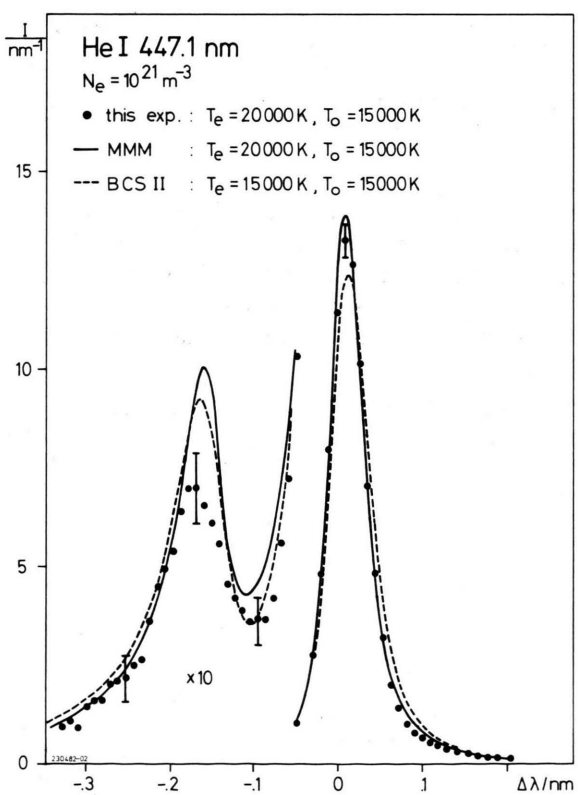

Fig. 9. Comparison of the measured line profile of 447.1 nm with BCS II and MMM at 1×10^{21} m^{-3}.

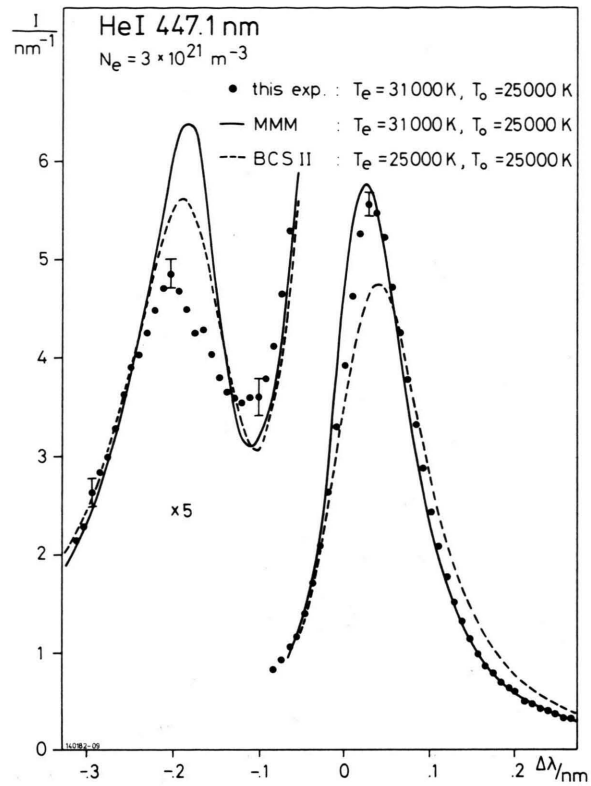

Fig. 10. Same as Fig. 9 but $N_e = 3 \times 10^{21}$ m^{-3}.

Figure 9 shows the line profile of 447.1 nm at $N_e = 1 \times 10^{21}$ m^{-3}. In this and the subsequent measurements $\Delta\lambda = 0$ corresponds to the unshifted position of the strongest member of the multiplet at 447.148 nm. The measured line profile exhibits a smaller intensity of the forbidden component than both theories. This difference clearly exceeds the error bar. The intensity of the valley agrees with that predicted by BCS II while the allowed line is better described by MMM with regard to the peak height and the line wing. The peak separation of allowed and forbidden line is slightly larger than predicted by MMM, but agrees with BCS II. The latter theory always shows a small red shift of both allowed and forbidden component.

Figure 10 shows the same line at $N_e = 3 \times 10^{21}$ m^{-3}. Again the forbidden component is weaker than both theories. The measured intensity of the valley is higher than the calculations and the allowed line is rather well described by MMM while BCS II shows larger deviations especially in the red wing. A similar tendency was observed in Figure 9.

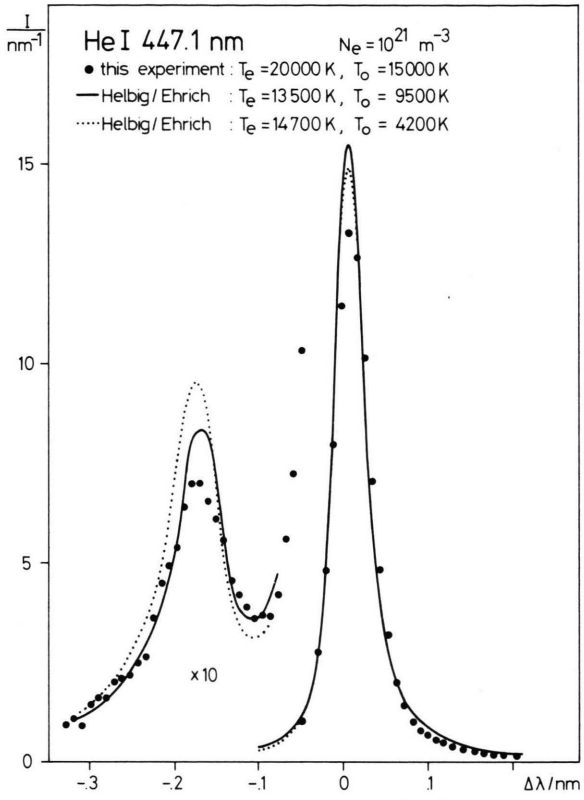

Fig. 11. Comparison with the experiments of Helbig and Ehrich [13] at 1×10^{21} m^{-3}.

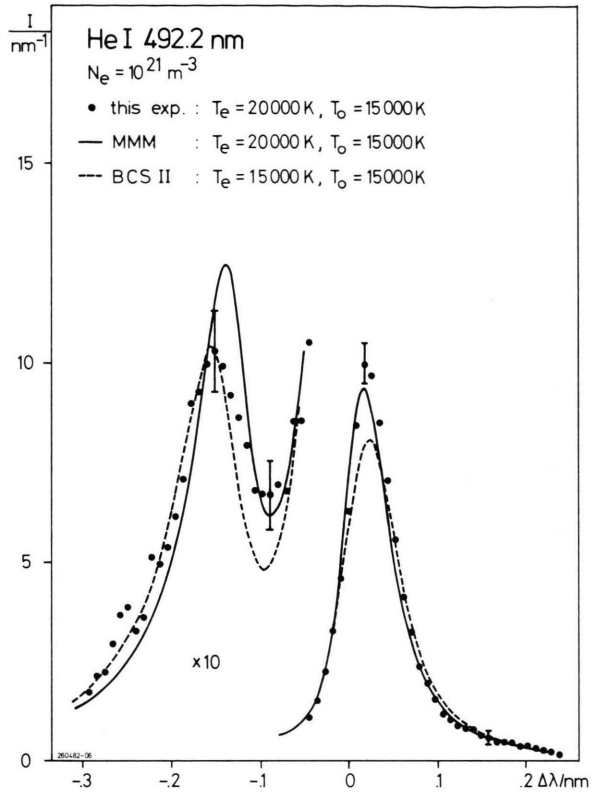

Fig. 12. Comparison of the measured line profile of 492.2 nm with BCS II and MMM at 1×10^{21} m^{-3}.

A comparison with the measurements of Helbig and Ehrich [13] is made in Figure 11. The electron density (1×10^{21} m^{-3}) was the same in all three measurements but the ion temperature varied from 4200 K to 15000 K. The tendency of a decreasing intensity of the forbidden component with increasing temperature is continued by our measurement, whereas the allowed line shows no monotonous trend. In our experiment the allowed line is smallest. The wings of all three measurements generally agree with each other.

Similar results have also been obtained for the line 492.2 nm, which is shown in Figure 12 for an electron density of 10^{21} m^{-3} and in Figure 13 for $N_e = 3 \times 10^{21}$ m^{-3}.

In Fig. 14 the line 492.2 nm is compared with the measurements of Helbig and Ehrich. From this comparison no monotonous tendency with increasing gas temperature can be concluded. The weak reduction in the peak height of the forbidden component lies within the experimental error. The allowed line at 15000 K is again lower than it was at 9500 K and confirms the finding of the 447.1 nm line. The line wings agree with each other.

We have found that in all our measurements the forbidden component is weaker than predicted by

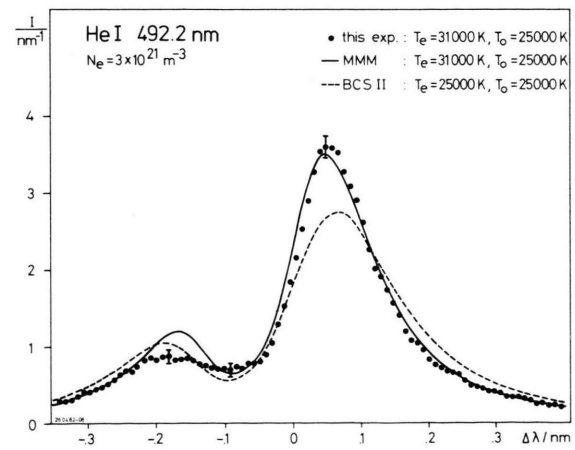

Fig. 13. Same as Fig. 12 but $N_e = 3 \times 10^{21}$ m^{-3}.

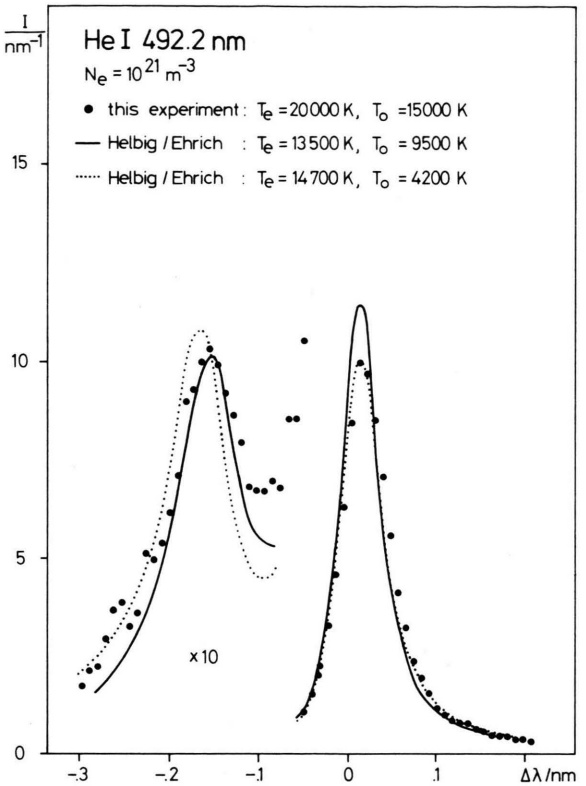

Fig. 14. Comparison of the measured line profile of 492.2 nm with the experiments of Helbig and Ehrich at 1×10^{21} m^{-3}.

the MMM theory. The allowed lines, however, are described fairly well by it. The BCS II calculations generally show lower peak intensities of both components due to a larger broadening. Unfortunately they are only tabulated for equal electron and gas temperatures. We have used the gas temperature for a comparison, since the electron temperature, which is only 24% higher, has only a negligible influence on the line shape, whereas comparing at T_e would increase the ion dynamics and Doppler broadening in the theory. Although BCS II gives a better description of the peak intensity of the forbidden component the deviations in the allowed line are remarkable, which is partly due to a red shift of both components. The separation of the peaks was always found slightly larger than predicted by the MMM theory but in better agreement with BCS II.

The trend found in the measurements of Helbig and Ehrich was only continued with regard to the intensity of the forbidden component, which monotonically decreases with increasing temperature. The narrowing of both components and the reduced peak separation of 447.1 nm at increasing temperature is not continued at a further increased temperature. The discrepancy in the allowed line can not be explained by the additional Doppler broadening.

An immediate comparison with the measurements of Fleurier et al. [11] has not been performed, since their profiles at $N_e = 3 \times 10^{21}$ m^{-3} are not normalized to unity area. Fleurier et al. [12] observed that in their experiments with hydrogen perturbers the line wings show an intensity 30% higher than with helium perturbers. The authors proposed an ion dynamic effect in the line wings, which is not accounted for in the theories yet. In our experiments no substantial variation of the wing intensity with the ion velocity could be observed. As pointed out above helium spectra suffer from superimposed hydrogen molecular lines, which also might explain the enlarged wing intensity.

IV. Summary

We have developed an improved plasma source of high purity for helium line profile measurements. The plasma parameters T_e, T_0 and N_e could be determined with sufficient accuracy by independent methods. As a first application we have investigated the line profiles of the overlapping helium lines $2\,^3P-4\,^3D$, ^3F and $2\,^1P-4\,^1D$, ^1F at low electron densities. In this regime ion dynamic effects considerably modify the line centers. The present measurements extend the gas temperature range investigated so far towards higher values.

In accordance with earlier observations the static ion profiles (BCS I) completely failed in explaining the experimental line shapes. Generally our line profiles are rather well described by the MMM theory. The BCS II profiles clearly deviate in the allowed line due to a larger broadening and red shift. The intensity of the forbidden line always was roughly 20% lower than the MMM calculations. This confirms the finding of Burgess and Cairns, who reported a forbidden component that was slightly lower than calculated by BCS II for the 447.1 nm line. The reduction in the forbidden line intensity with increasing gas temperature reported by Helbig and Ehrich is continued by our measurements. The peak separation of allowed and forbidden component of both lines exhibited a decreasing tendency

in the experiments of Helbig and Ehrich. This tendency is not continued by our result, which shows a peak separation that is nearly independent of ion temperature. In comparison with the theories this separation is larger than the value of MMM but in agreement with BCS II and Lee.

Acknowledgement

The authors wish to thank Dr. J. Seidel for providing unpublished tables of his MMM calculations of H_β. We are also grateful to Dr. G. Nollez for supplying us with Stark-broadening tables of the 447.1 nm and 492.2 nm lines at our experimental conditions. We thank Prof. H. Schlüter for his continuous interest in the progress of this work. The development of a pure helium discharge is a part of the Sonderforschungsbereich 162, Plasmaphysik Bochum-Jülich. The investigations of ion dynamic effects were financially supported by the "Ministerium für Wissenschaft und Forschung des Landes NRW".

[1] D. D. Burgess, J. Phys. B **3,** L70 (1970).
[2] D. D. Burgess and C. J. Cairns, J. Phys. B **3,** L67 (1970).
[3] H. R. Griem, Astrophys. J. **154,** 1111 (1968).
[4] A. J. Barnard, J. Cooper, and L. T. Shamey, Astron. Astrophys. **1,** 128 (1969).
[5] A. J. Barnard, J. Cooper, and E. W. Smith, J. Quant. Spectrosc. Radiat. Transfer **14,** 1025 (1974).
[6] R. W. Lee, J. Phys. B **5,** L23 (1972).
[7] R. W. Lee, J. Phys. B **6,** 1044 (1973)
[8] A. Brissaud, C. Goldbach, J. Leorat, A. Mazure, and G. Nollez, J. Phys. B **9,** 1147 (1976).
[9] G. Nollez, private communication.
[10] D. Voslamber and E. R. A. Segrè, J. Quant. Spectrosc. Radiat. Transfer **25,** 45 (1981).
[11] C. Fleurier, G. Coulaud, and J. Chapelle, Phys. Rev. A **18,** 575 (1978).
[12] C. Fleurier, G. Coulaud, and J. Chapelle, Physica **100 C,** 127 (1980).
[13] V. Helbig and H. Ehrich, in: Spectral Line Shapes, ed. B. Wende, p. 179–190, de Gruyter, Berlin 1981.
[14] A. Mazure, C. Goldbach, and G. Nollez, Z. Naturforsch. **34 a,** 773 (1979).
[15] H. Wulff, Z. Physik **150,** 614 (1958).
[16] J. Durant, thesis TH München published as Report Max-Planck-Institut MPI/PA/8/62 (1962).
[17] H. Wulff, Proc. VIIth Int. Conf. Ion. Phen. Gas., Beograde **1,** 829 (1965).
[18] H. W. Drawin and J. Ramette, Z. Naturforsch. **29 a,** 838 (1974).
[19] H. W. Drawin and J. Ramette, Z. Naturforsch. **33 a,** 1285 (1978).
[20] A. Piel and H. Richter, Z. Naturforsch. **34 a,** 516 (1979).
[21] A. Piel, in: Spectral Line Shapes, ed. B. Wende, p. 577–589, de Gruyter, Berlin 1981.
[22] D. E. T. F. Ashby and D. F. Jephcott, Appl. Phys. Lett. **3,** 13 (1963).
[23] J. B. Gerardo and J. T. Verdeyen, Appl. Phys. Lett. **3,** 121 (1963).
[24] A. Piel and H. Richter, Report Nr. 82-M2-098 (1982), Sonderforschungsbereich 162 Plasmaphysik Bochum-Jülich.
[25] J. Seidel, Z. Naturforsch. **32 a,** 1195 (1977).
[26] J. Seidel, Z. Naturforsch. **32 a,** 1207 (1977).
[27] J. Seidel, private communication.
[28] H. Ehrich and V. Helbig, J. Phys. B **12,** 1183 (1979).
[29] H. R. Griem, Spectral Line Broadening by Plasmas, Academic Press, New York 1974.
[30] H. R. Griem, Plasma Spectroscopy, McGraw Hill, New York 1964.
[31] D. R. Bates, A. E. Kingston, and R. W. P. Mc Whirter, Proc. Roy. Soc. **A 267,** 297 (1962).